Chemistry and Materials Research
ISSN 2224- 3224 (Print) ISSN 2225- 0956 (Online)
Vol 2, No.2, 2012

Composite integrated Material of Al layers with Kevlar material and the specification test result

Maria Antoine Pushparaj [1*] & Zeenath Fathima [2]

1. Mailam engineering college,Mailam,India

2. School of Mechanical Engineering,SRM University,Kattangulathur ,India

* E-mail of the corresponding author: pushparajmaria@gmail.com

Abstract

When the Kevlar material is used for the defense purpose and for the safety purpose at the time of the war enclosure the problem facing here is when the impact is applied at a point the material deformation occurs and at a particular point and the deflection will be very high so that the human who is wearing the Kevlar as the body proof experience a heavy pain in that , concluded is we are introducing a new composite material for the Kevlar design which will convert a point into a uniformly distributed load across the material hence by reducing the point deformation

Keywords: Shear thickening fluids (STFs), transmission electron microscopy (TEM)

1. Introduction

Kevlar is synthesized in solution from the monomers 1,4-phenylene-diamine (*para*-phenylenediamine) and terephthaloyl chloride in a condensation reaction yielding hydrochloric acid as a byproduct. The result has liquid-crystalline behavior, and mechanical drawing orients the polymer chains in the fiber's direction. Hexamethylphosphoramide (HMPA) was the solvent initially used for the polymerization, but for safety reasons, DuPont replaced it by a solution of *N*-methyl-pyrrolidone and calcium chloride. As this process was patented by Akzo (see above) in the production of Twaron, a patent war ensued.[9]phenylene-diamine (*para*-phenylenediamine) with terephthaloyl chloride yielding Kevlar.

Kevlar (poly paraphenylene terephthalamide) production is expensive because of the difficulties arising from using concentrated sulfuric acid, needed to keep the water-insoluble polymer in solution during its synthesis and spinning.

When reinforced with glass fiber, thermoplastics typically suffer a decrease in performance under humid conditions because of a lack of adhesion between the glass fibre and the resin. This challenge is key in many applications including appliance components, automotive under-the-hood and, in some case, consumer goods.

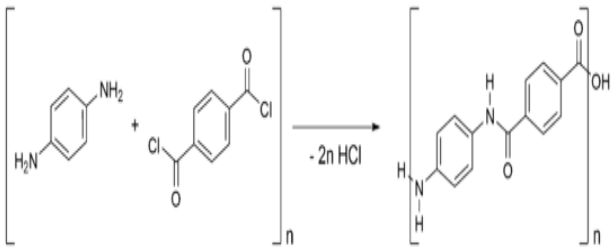

2. Grades of the Kevlar

1. *Kevlar K-29* – in industrial applications, such as cables, asbestos replacement, brake linings, and body/vehicle armor.
2. *Kevlar K49* – high modulus used in cable and rope products.
3. *Kevlar K100* – colored version of Kevlar
4. *Kevlar K119* – higher-elongation, flexible and more fatigue resistant.
5. *Kevlar K129* – higher tenacity for ballistic applications.

6. *Kevlar AP* – has 15% higher tensile strength than K-29
7. *Kevlar XP* – lighter weight resin and KM2 plus fiber combination.[11]
8. *Kevlar KM2* – enhanced ballistic resistance for armor applications[12]

3. Bullet proof vests

When a handgun bullet strikes body armor, it is caught in a "web" of very strong fibers. These fibers absorb and disperse the impact energy that is transmitted to the vest from the bullet, causing the bullet to deform or "mushroom." Additional energy is absorbed by each successive layer of material in the vest, until such time as the bullet has been stopped.

Because the fibers work together both in the individual layer and with other layers of material in the vest, a large area of the garment becomes involved in preventing the bullet from penetrating. This also helps in dissipating the forces which can cause no penetrating injuries (what is commonly referred to as "blunt trauma") to internal organs. Unfortunately, at this time no material exists that would allow a vest to be constructed from a single ply of material.

4. Different Materials Used

DuPont has developed law enforcement protection products for more than 25 years. Its Kevlar brand fiber, first developed in 1965, was the first material identified for use in the modern generation of concealable body armor. Kevlar is a manmade organic fiber, with a combination of properties allowing for high strength with low weight, high chemical resistance, and high cut resistance. Kevlar is also flame resistant; does not melt, soften, or flow; and the fiber is unaffected by immersion in water.

Another manufacturer, Akzo Nobel, has developed various forms of its aramid fiber TWARON for body armor. According to Akzo Nobel, this fiber uses 1,000 or more finely spun single filaments that act as an energy sponge, absorbing a bullet's impact and quickly dissipating its energy through engaged and adjacent fibers. Because more filaments are used, the impact is dispersed more quickly. Akzo claims their patented Microfilament technology allows maximum energy absorption at minimum weights while enhancing comfort and flexibility.

Akzo Nobel maintains that the use of TWARON in body armor significantly reduces the overall weight of the finished product, thus making vests more comfortable. Akzo also contends that stitching panels made from layers of TWARON is largely unnecessary, and that the lack of stitching contributes to a lighter weight and softer feel while affording the same protection.

Another fiber used to manufacture body armor is Dyneema. Originated in the Netherlands, Dyneema has an extremely high strength-to-weight ratio (a 1-mm-diameter rope of Dyneema can bear up to a 240-kg load), is light enough that it can float on water, and has high energy absorption characteristics.

Areal weight: 146 g / sq.m.
Weaving style: Plain
Width: 1.00 meters
Warp: Glass EC11-105 fiber, 54%, 7.5 ends (threads) / cm
Weft: Glass EC11-105 fiber, 46%, 6.4 ends (threads) / cm

5. Technical specification of Kevlar

Fibers of Kevlar consist of long molecular chains produced from poly-paraphenylene terephthalamide. The chains are highly oriented with strong interchange bonding, which results in a unique combination of properties.
General properties of Kevlar®:

- High Modulus
- High LASE (Load At Specified Elongation)
- High Tensile Strength at Low Weight
- Low Elongation to Break High Modulus (Structural Rigidity)
- Low Electrical Conductivity
- High Chemical Resistance
- Low Thermal Shrinkage
- High Toughness (Work-To-Break)
- Excellent Dimensional Stability
- High Cut Resistance
- Flame Resistant, Self-Extinguishing

6. Concepts of the composite development

A previous study investigated a related, but distinct effect to improve the performance of Kevlar woven fabrics. The used fibers coated with a dry powder that exhibits dilatants properties. In their work, the fibers demonstrated an improved ability to distribute energy during ballistic impact due to the enhanced interfiles friction. The objective of this study is to investigate the ballistic properties of woven Kevlar fabrics impregnated with fluids that exhibit the shear thickening effect. At low strain rates, associated with normal motion of the wearer, the fluid will offer little impediment to fabric flexure and deformation. However, at the high strain rates associated with a ballistic impact event, the fluid will thicken and in doing so, enhance the ballistic protection of the fabric. The results of this study confirm these hypotheses, and demonstrate that the novel composite material could provide a more flexible, and less bulky, alternative to neat Kevlar fabrics.

7. Experimental Materials

The colloidal silica used to produce the shear thickening fluids (STFs) for this investigation (Nissan Chemicals (MP4540)) is provided as an aqueous suspension at a particle concentration of about 40 wt%. The particle size was characterized with dynamic light scattering and transmission electron microscopy (TEM). Fig. 1 shows the TEM micrographs of a dried sample of the dispersion. The particles are bimodal in size, with a minor fraction of smaller particles. The average particle diameter was determined to be 446 nm by dynamic light scattering. The density of the silica particles was Transmission electron microscopy of colloidal silica obtained from Nissan Chemicals (MP4540) at a magnification of 40,000. calculated from density measurements (DMA 48 density meter (Anton Paar)) conducted on dilute samples of the dispersion. The weight fraction of silica in each solution was measured by drying in a convection oven at 180◦C for 5 h and weighing the residual dry silica. From the mass fraction, solvent density and the corresponding measured solution density, the density of the silica particles in solution was estimated to be 1.78 g/cc.

As a means of preparing a stable, shear thickening concentrated dispersion, the aqueous medium was replaced with ethylene glycol. Ethylene glycol was chosen as a solvent due to its low volatility and thermal stability. Additionally, the index of refraction of ethylene glycol is close to that of the silica particles, providing enhanced colloidal stability. Three hours of centrifugation at 3,900 rpm using a table top centrifuge (IEC clinical centrifuge) was performed to separate the silica particles from the aqueous-based supernatant. The silica sediment was then crushed using a spatula and re suspended in ethylene glycol using a vortex mixer. This process was repeated 4 times in order to minimize the amount of residual aqueous supernatant present within the samples. The final weight fraction of particles in this stock solution was determined by using a moisture analyzer (Mettle Toledo, HR73).

Rheological measurements were performed primarily with a stress-controlled rheometer.To (SR-500, Rheumatics) at 25◦C with cone-plate geometry having a cone angle of 0.1 radian and a diameter of 25 mm. Complementary measurements were performed on a Rheumatics ARE Controlled strain rheometer.To minimize the effects of solvent evaporation during testing, a solvent trap was used during all remoter measurements. To remove sample loading effects, a preheat of 1 s−1 was applied for 60 s prior to further measurement. All measurements presented here were reproducible.

7.1 Kevlar fabric

The Kevlar fabric used in all composite target constructions was plain-woven Hexcel Aramid (polyparaphenylene terephthalamide), high performance fabric Style 706 (Kevlar KM-2, 600 denier) with an areal density of 180 g/m2.

8. Target preparation

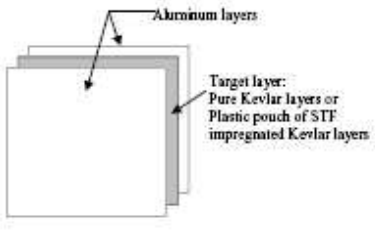

Ethylene glycol (surface tension = 47.7 dyne/cm) was observed to wet the Kevlar fabric. To facilitate impregnation of the STF into the Kevlar fabric, an equal volume of ethanol surface tension (22.0 dyne/cm) was added to the original ethylene glycol based STF. This diluted STF was observed to spontaneously impregnate the fabric. Following impregnation, the composite fabric was heated at 80◦C for 20 min in a convection oven to remove the ethanol from the sample. The final composition of the impregnated STF is 57 vol% silica in ethylene the ethylene glycol was removed prior to imaging by

drying the sample at 200◦C for 24 h, leaving only the silica particles and Kevlar fabric. The image shows silica particles dispersed within the yarn, 2826 demonstrating that the original STF was fully impregnated between the individual Kevlar fibers within each yarn. In addition to the STF-impregnated fabric, samples were made of fabric impregnated with neat ethylene glycol.

The ethylene glycol-impregnated fabric was made using the same ethanol dilution and evaporation method used for the STF-impregnated targets is a schematic diagram of a ballistic target. Two pieces of 5.08 cm × 5.08 cm aluminum foil (1mm thickness) were used to encapsulate the targets. The Kevlar layers were cut to 4.76 cm × 4.76 cm, impregnated with varying amounts of STF per layer (2, 4, and 8 ml) as indicated, and then assembled into the targets by stacking them to the desired target configuration.

To prevent leakage of STF out of the target assembly and because Kevlar is known be sensitive to moisture, heat-sealed polyethylene film (Zip lock bags sealed using a ULINE KF-200HC heat sealer) was used to encapsulate the targets. Neither the aluminum foil nor the polyethylene packaging provided any measurable ballistic resistance.

These targets were mounted onto a single ply of unimpregnated Kevlar, glued to a 5.08 cm diameter copper hoop (0.635 cm wire diameter) using Liquid Nails adhesive (ICI), in order to help support the target during testing. In all cases this mounted Kevlar layer was immediately adjacent to the ballistic target, with the copper hoop resting inside of the target mounting frame. All subsequent descriptions of ballistic targets will list only the Kevlar layers within the aluminum foil layers, and do not include this individual backing Kevlar layer.

8.1 Ballistic tests

The ballistic tests were performed using a smooth bore helium gas gun (Army Research Laboratory, MD). All tests were performed at room temperature. The gun was sighted on the target center and the impact velocity was adjusted to approximately 244 m/s (800 fps). The exact impact velocity of each projectile was measured with a chronograph immediately before impacting the target. The projectile is a NATO standard fragment simulation projectile (FSP), consisting of a chisel-pointed metal cylinder of 1.1 grams (17 grains) and 0.56 cm diameter (22 caliber). A 10.16 cm × 10.16 cm × 2.54 cm thick aluminum block was cut with a recessed square hole to accept the 5.08 cm square target package
The target was held in place using light pressure from spring clips located along its edge. The mounting block was then clamped onto a steel frame in line with the gas gun barrel. A clay witness was used to measure the depth of indentation Modeling clay (Van Aken International) was packed into a 15.24 cm × 8.89 cm × 8.89 cm wooden mold, compressed with a mallet, and cut into four 7.62 cm × 4.45 cm square pieces. This process minimizes air bubbles or poor compaction in the clay witness. The molded clay block was held onto the back of the target using a strip of adhesive tape.

In order to normalize results with respect to variations in impact velocities, ballistic test results are also presented in terms of dissipated projectile kinetic

$$E = \frac{1}{2} m_p \left(V_i^2 - V_r^2 \right)$$

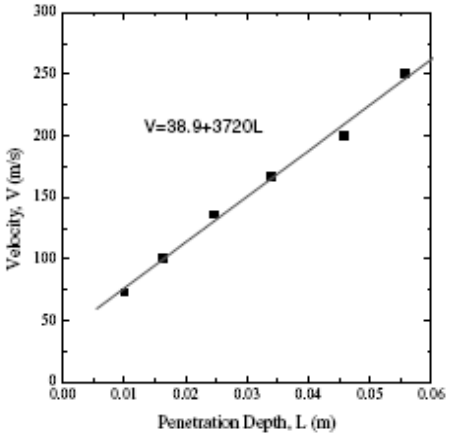

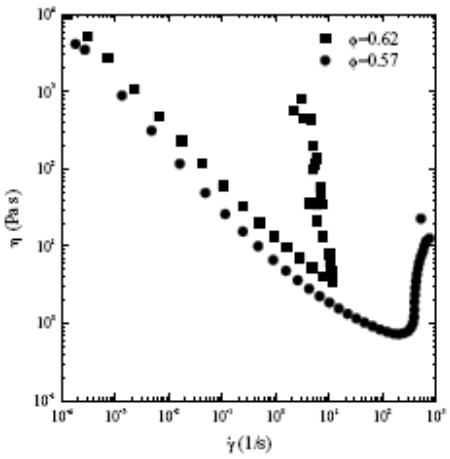

schematic diagram of ballistic experimental setup. where E is the dissipated energy (J), mp is the projectile mass (kg), Vi is the initial projectile velocity (m/s), and Vr is the residual velocity of the projectile after penetrating the target (m/s).In order to relate depth of penetration to residual projectile velocity, a series of experiments were performed using an empty target frame and clay witness resulting penetration depth as a function of projectile velocity, which is closely modeled by the linear relationship

$$V\text{r} = 38.9 + 3720\,L$$

Where L (m) is the penetration depth into the clay witness. Equations 1 and 2 are used throughout this paper to relate depth of penetration to residual projectile kinetic energy. The energy dissipated by the target is normalized by the initial kinetic energy of the projectile to obtain the fractional dissipation.

Velocity, V (m/s)

Penetration Depth, L (m)

8.2 Flexibility and thickness tests

Two-dimensional drape tests were performed to measure the flexibility of the targets, in all cases a 20 g weight was used, and encapsulated ballistic targets were used as the test specimens. Bending angle is reported as a measure of target flexibility, with larger angles indicating greater flexibility. Target thickness at the center of the targets was also measured with a micrometer.

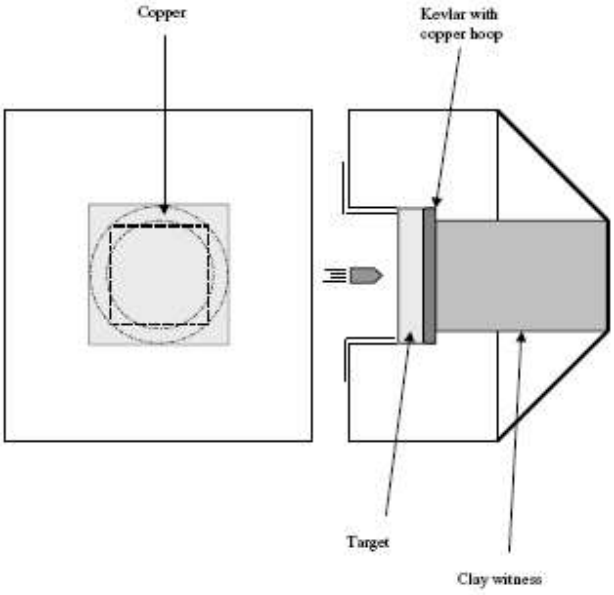

8.3 Results Rheological properties of shear thickening suspension

The steady shear viscosity as a function of the steady shear rate for the ethylene glycol based silica suspension at volume fractions of φ = 0.57 and 0.62. Note that the data are collected on a controlled stress remoter where an applied shear stress is controlled and the corresponding shear rates measured. However, the data has been plotted against the measured shear rate rather than the applied stress, as is more traditional. The use of controlled stress enables probing the regime of extreme shear thickening observed at high shear rates, which is not possible in a controlled rate device due to the nature of the material's response. Both shear thinning and shear thickening behavior are observed. At these high particle loadings, the silica suspensions are glassy at rest and yield at low shear rates. This manifests in Fig. 7 as strong shear thinning $\eta(\dot{\gamma}) \propto \dot{\gamma} - 1$, which is a signature of a yield stress th increasing shear rate the viscosity begins to plateau, followed by a transition to shear thickening behavior at high shear rates. The shear thickening transition was observed to occur at shear rate of 10 s−1 for the concentrated dispersion having a particle volume fraction of φ = 0.62 and 300 s−1 for the fluid with a particle volume fraction of φ = 0.57. At high shear rates in the shear thickening region, the high volume fraction (φ =0.62) dispersion exhibits a greater increase in viscosity. Transducer limitations and sample adhesive failure to the tooling silica dispersed in ethylene glycol for steady shear flow. prevented exploration of higher shear stresses. However, careful analysis of the slip in these materials [20, 25] demonstrates that the sample solidifies in the shear thickened regime, such that the reported viscosities.

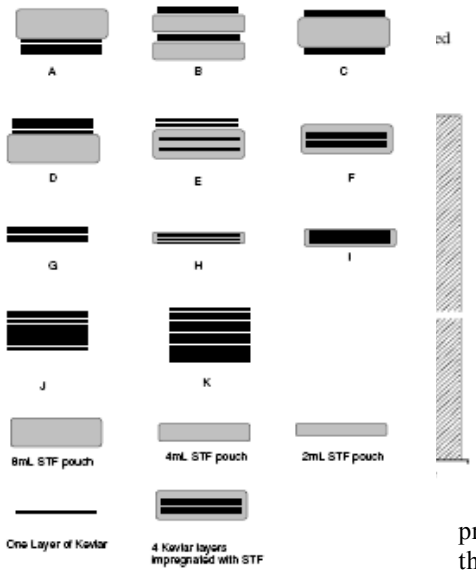

After the onset of shear thickening are more representative of the suspension slipping against the tooling. Note also that the shear thickening transition is reversible, i.e., this liquid-to-solid transition induced by flow is not associated with particle aggregation, nor it results in any irreversible change in the dispersion. This effect is shown in as the data plotted corresponds to both ascending and descending shear stresses without hysteresis. The shear thickening transition in colloidal dispersions is believed to result from a micro structural change where the hydrodynamic forces overcome antiparticle forces to create particle clusters [26]. These cluster formations, referred to as "hydro clusters," increase the hydrodynamic stress in the suspension, thus marking the onset of shear thickening. The hydro clustered state, however, does not lead to permanent or irreversible particle aggregation. Additional rheological studies have shown that the timescales for this transition are on the order of millisecond or less [15, 20, 25].The characteristic shear rate for the ballistic testing performed here is estimated to be on the order of 45,000 1/s ($\dot{\gamma} = vx/y = 24400/0.56$), based on a projectile velocity of 800 fps (244 m/s) and a projectile diameter of 22 caliber (0.56 cm). This shear rate greatly exceeds the rate required for the onset of shear thickening in this fluid (about 300 1/s for the silica suspension with $\varphi = 0.57$). Thus we expect the shear rates during the ballistic tests to be sufficient to transition the dispersion to its shear thickened state.

8.4 Ballistic test results

TABLE I Test results of samples with 4 layers of Kevlar and 8 ml of shear thickening fluid with different configurations but equal target weights

Target	Description	Sample weight (g)	Impact velocity (m/s)	Penetration depth (cm)	Dissipated energy (Joule)
A	8 ml STF-K-K-K-K	13.9	247	1.72	27.8
B	K-K-4 ml STF-K-K-4 ml STF	13.9	249	1.36	29.8
C	K-K-8 ml STF-K-K	13.9	244	1.22	28.9
D	K-K-K-K-8 ml STF	13.9	253	1.19	31.5
E	K-K-8 ml STF impregnated in 2 layers of Kevlar	13.9	242	0.787	29.7
F	8 ml STF impregnated in 4 layers of Kevlar	13.9	253	0.673	32.9

The ballistic test results of a series of targets composed of 4 layers of Kevlar and 8 ml of STF with different configurations (targets A to F in Fig. 8) are shown in Figs 9–11 and summarized in Table I. The projectile has been stopped in all targets. Fig. 9 shows the energy dissipation for these targets, with the fully impregnated targets (E, F) showing significantly less penetration depth than the unimpregnated targets (A, B, C, D). The clay witness penetration profiles (Fig. 10) also show a marked difference in shape, as the unimpregnated targets show sharp, deep penetration profiles, while the impregnated samples show a blunt, shallow impregnation. These results clearly show that impregnating the STF into the fabric is critical to achieving an enhancement in the fabric ballistic properties. Shows the front Kevlar layers for targets D(Unimpregnated) and F (impregnated). The unimpregnated target shows that the Kevlar yarns that were directly impacted by the projectile pullout significantly from the weave, producing the well-documented cross pattern in the fabric.

Note that the Kevlar layers exhibit little actual fiber breakage, although some fiber stretching near the impact point may have occurred. In contrast, the first layer of Kevlar in the impregnated target shows extensive fiber breakage near the projectile
contact point, and only very little yarn pullout or wrinkling in the surrounding fabric. Some fiber stretching may have occurred at the impact point. Note that yarn pullout is evident only for the yarns directly impacted by the projectile, with the total pullout distance significantly less than that observed for the neat Kevlar target. Having demonstrated that fabric impregnation is essential to realizing enhanced performance; further targets were constructed to establish the scaling of energy absorption with the relative amount of STF and Kevlar in the target. Table II and Fig. 12 show the energy dissipated by targets consisting of 4 impregnated layers of
Fabric, as a function of the volume of STF. As shown in this figure, the energy absorption by the target increases continuously with the total volume of STF in the target. To demonstrate that the enhanced ballistic performance of the impregnated fabrics is not simply a consequence of increased target mass or solvent effects on the Kevlar weave tests were performed using Kevlar that was impregnated with pure ethylene glycol. As shown in Fig. 12, samples of ethylene glycol-impregnated Kevlar show relatively poor ballistic performance compared with STF-impregnated Kevlar with equal impregnated fluid volume. In this graph, the dotted line shows the amount of energy dissipated by 4 layers of pure Kevlar

(target G). The results show that the addition of ethylene glycol does not improve the impact energy absorption capacity of Kevlar fabric. In fact, at high loadings (8 ml ethylene glycol) the performance is even worse than neat Kevlar, despite the increased target mass. This decrease in performance may be due to lubrication effects, as the solvent (which is Newtonian at these shear rates, unlike the shear thickening fluid) may reduce the friction between fibers in the fabric during yarn pullout.
A direct comparison between the ballistic protection performance of targets consisting of pure Kevlar fabric and STF-impregnated Kevlar fabric with nearly equal total weight has been made in Table III and Fig. 13. As shown in Fig. 13, the composite, impregnated targets have the same ballistic resistance as targets of equal than the number of Kevlar layers in the neat Kevlar targets.

Target	Description	Sample weight (g)	Penetration depth (cm)	Dissipated energy (Joule)	Bending angle, θ (°)	Sample thickness (mm)
G	4 layers of Kevlar	1.9	2.12	25.1	50	1.4
J	10 layers of Kevlar	4.7	1.55	28.6	13	3.0
H	2 ml STF impregnated in 4 layers of Kevlar	4.8	1.23	28.6	51	1.5

8.5 Flexibility and thickness test results

The test results for the flexibility of 4 layers of Kevlar, 10 layers of Kevlar and 4 layers of Kevlar impregnated with 2 ml STF are presented in Table IV. The weight and ballistic performance of the 4-layer STF impregnated Kevlar is nearly the same as that of the10-layer unimpregnated Kevlar. However, the 4-layer STF-impregnated Kevlar is more flexible (bending angle = 51◦) than the 10-layer unimpregnated Kevlar (bending angle = 13◦) with same overall weight. In fact, there is no difference in flexibility between them .

9. Discussion

The results clearly demonstrate that, under our test conditions, impregnating neat Kevlar fabric with STF enhances the ballistic properties of the fabric. More precisely, the addition of STF to the fabric increases the amount of projectile energy that is absorbed by the target. A number of possible mechanisms could explain this behavior. Fig. 11 shows that the impregnated fabric exhibits significantly less pullout that the unimpregnated fabric, both in terms of the number of yarns pulled and the pullout distance per yarn. The impregnated target, unlike the neat fabric, also exhibits significant fiber fracture at the impact point. Anotherimportant difference is that all four layers of fabric in target D (not shown) exhibited extensive pullout, comparable to that of the first layer of fabric. In contrast, the three backing layers of target F (not shown) exhibited little or no pullout, and no fiber fracture. Therefore, most of the energy absorption in the impregnated target was likely provided by the first layer of Kevlar, although the backing layers may still have provided a critical secondary role during the impact event. These results suggest that the STF constrains the Kevlar yarns as they are pulled through the fabric. The increase in energy dissipation in the impregnated target could be due in part to an increase in force required to pullout each yarn from the fabric, so that less totalpullout is required to absorb the projectile energy. An alternative explanation is that the increased pullout resistance increases the loads on the yarns during impact which then absorb additional energy through fiber deformation and fracture. To address these issues, we are performing additional ballistic tests at higher velocities, and performing quasistatic yarn pullout tests [3,27] with and without STF.

10. Conclusions and future work

This study demonstrates that the ballistic penetration resistance of Kevlar fabric is enhanced by impregnation of the fabric with a colloidal shear thickening fluid. Impregnated STF-fabric composites are shown to provide superior ballistic protection as compared with simple stacks of neat fabric and STF. Comparisons with fabrics impregnated with non-shear thickening fluids show that the shear thickening effect is critical to achieving enhanced performance. Energy absorption by the STF-fabric composite is found to be proportional to the volume of STF. Compared with neat Kevlar fabrics of equivalent weight, the STF-impregnated Kevlar fabric provides nearly the same ballistic protection, yet is much thinner and more flexible.

References

Ausiello, P., Apicella, A., Davidson, C. L. (2002). Effect of adhesive layer on stress distribution in composite restorations – a 3D finite element analysis, Dental Materials, 18, 295-303.
Beckert, W., Lauke, B. (1995). Fracture mechanics finite element analysis of debonding crack extension for a single fibre pull-out specimen, J. Mat. Sci. Lett., 14, 333-336.
Boisse, P., Borr, M., Buet, K., Cherouat, A. (1997). Finite element simulations of textile composite formed including the biaxial fabric behavior, Comp. B, Eng., 28, 453-464.
Butcher, R. J., Rousseau, C. E., Tippur, H. V. (1999). A functionally graded particulate composite: Preparation, Measurements and failure analysis, Acta Mater. 47, 259-268.
Chang, F. K., Scott, R. A., Springer, G. S. (1982). Strength of mechanically fastened composite joints, J. Comp. Mat. 16, 470-494.
Change, F. K., Chang, K. Y. (1987). A progressive damage model for laminated composites containing stress concentrations, J. Comp. Mat., 21, 834-855.
Chen, X., Liu, Y. (2001). Multiple-cell modelling of fibre-reinforced composites with the presence of interphases using the boundary element method, Comp. Mat. Sci. 21, 86-94.
Choo, H., Bourke, M. A. M., Daymond, M. R. (2001). A finite-element analysis of the inelastic relaxation of thermal residual stress in continuous-fiber-reinforced composites, Comp. Sci. Tech., 61, 1757-1722.
Davies, G. A. O., Zhang, X., Zhou, G., Watson, S. (1994). Numerical modelling of impact damage, Composites, 25, 342-350.
Dehoff, P. H., Anusavice, W. J., Wang, Z. (1995). Three-dimensional finite element analysis of the shear bond test, Dent. Mater., 11, 126-31.
Diaz, J., Romera, L., Hernandez, S., Baldomir, A. (2010). Benchmarking of three-dimensional finite element models of CFRP single-lap bonded joints, Int. J. Adhesion and Adhesives, 30, 178-189.
312 Finite Element Analysis
Dooms, D., Degrande, G., Roeck, G. D., Reynders, E. (2006). Finite element modelling of a silo based experimental nodal analysis, Eng. Structures, 28, 532-542.
Fisher, F. T., Bradshaw, R. D., Brinson, L. C. (2003). Fiber waviness in nanotube-reinforced polymer composites—II: modeling via numerical approximation of the dilute strain concentration tensor, Comp. Sci. Tech., 63, 1705-1722.
Fisher, F. T., Brinson, L. C. (2001). Viscoelastic interphases in polymer-matrix composites: Theoretical models and finite element analysis, Composites Sci. and Tech. 61, 731-748.
Gamble, K., Pilling, M., Wilson, A. (1995). An automated finite element analysis of the initiation and growth of damage in carbon-fibre composite materials, Comp. Structures, 32, 265-274.
Guild, F. J., Young, R. J. (1989). A predictive model for particulate-filled composite materials, J. Mat. Sci., 24, 298-306.
Houshyar, S., Hodzic, A., Shanks, R. A. (2009). Modelling of polypropylene fibre-matrix composites using finite element analysis, eXPRESS Polymer Letters, 3, 2-12.
Houshyar, S., Shanks, R. A. (2003). Morphology, thermal and mechanical properties of poly(propylene) fibre-matrix composites, Macromol. Mat. Eng., 288, 599-606.
Houshyar, S., Shanks, R. A. (2010). Interfacial properties of all-polypropylene composites, e-Polymers, 33, 1-13.
Houshyar, S., Shanks, R. A., Hodzic, A. (2005). The effect of fiber concentration on mechanical and thermal properties of fiber-reinforced polypropylene composites, J. Appl. Polym. Sci., 96, 2260-2272.
Huang A., Bush M. B. (1997). Finite element analysis of mechanical properties in discontinuously reinforced metal matrix composites with ultra fine micro structure. Mat. Sci. Eng. A, 232, 63–72.

Hutchinson, J. W., Jensen, H. M. (1990). Models of fiber debonding and pullout in brittle composites with friction, Mecahnical of Materials, 9,139-163.
Hyung, Y. C., Wu, H. Y. T., Fu-Kuo, C. (1991). A new approach toward understanding damage mechanisms and mechanics of laminated composites due to low-velocity impact. II: analysis, J. Comp. Mat., 25, 1012-1038.
Isakson, G., Levy, A. (1971). Finite element analysis of interlaminar shear in fibrous composites, J. Comp. Mat., 5, 273-276.
Kang G. Z., Gao Q. (2002). Tensile properties of randomly oriented short Al2O3 fibre reinforced aluminium alloy composites: II. Finite element analysis for stress transfer, elastic modulus and stress-strain curve. Composites A, Appl. Sci. Manufacturing, 33, 657–667.
Lamkanfi, E., Paepegem, W. V., Degrieck, J., Ramault C. (2010). Strain distribution in cruciform speciments subjected to biaxial loading conditions. Part 1. Twodimensional finite element model, Polym. Testing, 29, 7-13.
Lee, S. H., Wang, S., Pharr, G. M., Xu, H. (2007). Evaluation of interphase properties in a cellulose fiber-reinforced polypropylene composite by nanoindentation and finite element analysis, Composites A, 38, 1517-1524.
Lim, J. H., Ratnam, M. M., Abdul-Khalil H. P. S (2003). An experimental and finite element analysis of the static deformation of natural fiber-reinforced composite beam, Polym. Testing, 22, 169-177.
Modelling of polymeric fibre-composites and finite element simulation of mechanical properties 313
Lin, D. X., Ni, R. G., Adams, R. D. (1984). Prediction and measurement of the vibrational damping parameers of carbon and glass fire-reinforced plastics plates, J. Comp. Mat., 18, 132-152.
McCarthy, M. A., McCarthy, C. T. (2002). Finite element analysis of the effects of clearance on single-shear, composite bolted joints, J. Plastics, Rubber Comp., 32, 1-11.
Maligno A. R., Warrior N. A., Long A. C. (2008). Finite element investigations on the microstructure of fibre reinforced composites. Express Polymer Letters, 2, 665–676.
Muheim, D., Griffen, O. H. (1990). 2-D to 3-D global/local finite element analysis of crossply composite laminates, J. Reinforced Plastics Comp., 9, 492-502.
Naik, N. K., Shembekar, P. S. (1992). Elastic behaviour of woven fabric composites: I – lamina analysis, J. Comp. Mat.,26, 2196-2225.
Nakamura, T., Imanishi, A., Kashima, H., Ohyama, T., Ishigaki, S. (2001), Stress analysis of metal-free polymer crowns using the three-dimensional finite element method, Int. J. Prosthodont, 14, 401-405.
Nedele, M. R., Wisdom, M. R. (1994). Three-dimensional finite element analysis of the stress concentration at a single break, Comp. Sci. Tech., 51, 517-524.
Pal, P., Ray, C. (2002). Progressive failure analysis of laminated composite plates by finite element method, J. Reiforced Plastics and Composites, 21, 1505-1513.
Pavier, M. J., Clarke, M. P. (1996). Finite element prediction of the post-impact compressive strength of fibre composites, Comp. Structures, 36, 141-153.
Pegoretti, A., Fambri, L., Zappini, G., Bianchetti, M. (2002). Finite element analysis of a glass fibre reinforced composite endoplastic post, Biomaterials, 23, 2667-2682.
Shati F. K., Esat I. I., Bahai H. (2001). FEA modelling of visco-plastic behaviour of metal matrix composites. Finite Elements in Analysis and Design, 37, 263–272.
Song, Y. S., Youn, J. R. (2006). Evaluation of the effective thermal conductivity for carbon nanotube/polymer composites using control volume finite element method, Carbon, 44,710-717.
Soykasap, O. (2010). Finite element analysis of plain weave composites for flexural failure, Polym. Composites, 31, 581-586.
Sun, C. T., Chen, J. K. (1985). On the impact of initially stressed composite laminates, J. Comp. Mat., 19, 490-504.
Tan, P., Tong, L., Steven, G. P. (1998). Modelling approaches for 3D orthogonal woven composites, J. Reinforced Plastics Comp., 17, 545-577.